Journal of Magnetism and Magnetic Materials 321 (2009) 1452–1458

Contents lists available at ScienceDirect

Journal of Magnetism and Magnetic Materials

journal homepage: www.elsevier.com/locate/jmmm

Formation and properties of magnetic chains for 100 nm nanoparticles used in separations of molecules and cells

Robert J. Wilson [a,*], Wei Hu [a], Cheryl Wong Po Fu [a], Ai Leen Koh [a], Richard S. Gaster [a], Christopher M. Earhart [a], Aihua Fu [a], Sarah C. Heilshorn [a], Robert Sinclair [a], Shan X. Wang [a,b]

[a] Department of Materials Science and Engineering, Stanford University, Stanford, CA 94305, USA
[b] Department of Electrical Engineering, Stanford University, Stanford, CA 94305, USA

ARTICLE INFO

Available online 20 February 2009

Keywords:
Magnetic nanoparticle
Nanoparticle characterization
Biomedical application
Bimetallic nanoparticle
Magnetic property

ABSTRACT

Optical observations of 100 nm metallic magnetic nanoparticles are used to study their magnetic field induced self assembly. Chains with lengths of tens of microns are observed to form within minutes at nanoparticle concentrations 10^{10}/mL. Chain rotation and magnetophoresis are readily observed, and SEM reveals that long chains are not simple single particle filaments. Similar chains are detected for several 100 nm commercial bio-separation nanoparticles. We demonstrate the staged magnetic condensation of different types of nanoparticles into composite structures and show that magnetic chains bind to immuno-magnetically labeled cells, serving as temporary handles which allow novel magnetic cell manipulations.

Magnetic nanoparticles are widely used in biology and medicine for applications which include biomolecule purification and cell separation [1], magnetic resonance imaging (MRI) contrast agents [2], and bio-magnetic sensors [3]. There is also much recent interest in magnetic hyperthermia [4] and magnetically targeted delivery [5] and transfection [6]. In all of these applications the magnetic field induced aggregation of particles can have strong effects by altering interparticle distances and creating clusters which are subject to size- and shape-dependent forces. Understanding the basis of cluster formation and the resulting modifications to composite particle behavior is therefore important to a broad range of phenomena. Although the formation and properties of magnetic chains are well documented for micron-sized particles [7], direct real space observation of particle assembly becomes difficult when particle diameters are reduced to the nanometer scale. As a result, even the existence of magnetic chains can become uncertain.

We, therefore, initiated studies to observe the formation and properties of magnetic chains composed of 100 nm metallic magnetic nanoparticles. Our initial interests included the basic formation of chains and their magnetophoretic velocities and viscous drag forces, which are helpful for understanding the effects of chaining on magnetic separation and retention. In the course of these studies, we found that we could observe chains in many commercial 100 nm magnetic reagents, including MagCellect (MC) [8] (Immunicon, R&D systems), 130 nm diameter Nanomag D [9] (microMod) and Feridex [10] (Berlex). Each of these types of nanoparticles has high iron oxide content and diameters near 100 nm. We examined mixtures of MagCellect and synthetic antiferromagnetic (SAF) nanoparticles [11], which exhibit chain formation at different magnetic fields, to show that composite structures, which involve magnetically staged condensation of both types of nanoparticles, can be obtained. Finally, we observed that chains magnetically reversibly bind to immuno-magnetically labeled cells, and can enhance the cell's magnetic responsiveness and allow novel magnetic manipulations.

The optical observations of individual magnetic nanoparticles that are reported here were enabled by our development of a novel type of highly magnetic nanoparticle [11], which is fabricated from pure metals and strongly scatters light. These monodisperse synthetic antiferromagnetic nanoparticles were made using layered metal films deposited on substrates which are pre-patterned using nanoimprint lithography. Details of fabrication, magnetic characteristics, and electron microscopy observations of dimensions and layer structure are available elsewhere [11–14]. The layer structure of the 100 nm diameter metal nanoparticles used in this work is 5 Ta/2 Ru/10 $Co_{90}Fe_{10}$/2.5 Ru/10 $Co_{90}Fe_{10}$/2 Ru/5 Ta, where the notation gives the thickness, in nm, and elemental composition of the layers. Tantalum is used as a protective layer, ruthenium is used to control intra-layer magnetic interactions, and a cobalt iron alloy provides high magnetic moment (1500 emu/cc). These SAF exhibit zero remanence, a linear low-field response, and adjustable magnetic saturation fields. The magnetic moment of the particles is

* Corresponding author at: Stanford University, Geballe Laboratory for Advanced Materials, 234 McCullough Building, 476 Lomita Mall, Stanford, CA 94305-4045, USA. Tel.: +1 650 724 3686; fax: +1 650 736 1984.
E-mail address: RobertJ.Wilson@stanford.edu (R.J. Wilson).

0304-8853/$ - see front matter © 2009 Elsevier B.V. All rights reserved.
doi:10.1016/j.jmmm.2009.02.066

deliberately made comparable to those of 100 nm spherical iron oxide particles by using thin $Co_{90}Fe_{10}$ layers.

These nanoparticles can be directly viewed using reflected light optical microscopy with a high numerical aperture (NA) immersion objective lens, even though the nanoparticle size is well below the diffraction limit. The high NA requirement results in a focal depth of field of only a few microns, and optical working distances near 100 μm require thin sample cells. Thus, these measurements are performed with immersion or on liquid samples between a cover slip and, typically, a 20 μm deep chamber slide (Hamilton–Thorne). Beneath the slide is a 1 in diameter, 1 in long cylindrical Alnico permanent magnet, magnetized along the cylinder axis, which can be rotated and translated relative to the slide. When the magnet is horizontal and centered under the objective, the magnetic field is also horizontal and has no horizontal gradient. Horizontal gradients are obtained by translating the magnet off center. In this geometry [15], there is always a vertical field gradient, and particles always seek the high fields produced near the magnet. All images were extracted from videos which may be viewed [15].

For studies of cell–chain interactions, human umbilical vein endothelial cells (HUVEC) [16] were grown from frozen samples through several generations using EDTA-mediated passages on 4 in culture plates. Harvested cells were washed repeatedly using 300 g centrifugation for 5 min to form pellets, followed by aspiration and resuspension in PBS buffer. The washed HUVEC were then labeled with biotinylated antibody, as per the supplier's protocol, using a PlusCellect kit (R&D Systems) targeting platelet endothelial cellular adhesion molecule (PECAM1, CD31) surface markers. After this incubation, streptavidin-coated MagCellect nanoparticles were added for a second incubation, after which the labeled cells were washed repeatedly to remove excess antibody and nanoparticles. To study chain–cell interactions, magnetic nanoparticles were added back to the washed labeled cell sample, or washing steps were omitted.

Single 100 nm metal particles can be easily tracked within an optical cell provided their vertical range is small enough that diffusing particles cannot leave the few micron focal depth. In deeper cells these nanoparticles, with diffusion constants 2 $\mu m^2/s$, move through the focal depth in about a second and appear as flickering dots in image streams [15] captured with 40 ms exposures and 2 Hz frame rates. SEM and optical counting of particles confirm that most SAF are present as individual particles when no magnetic field is applied. Fig. 1a shows an image of these diffusing nanoparticles in zero field at a concentration 10^{10}/mL. When the magnetic field is increased to 1 kOe, the nanoparticles magnetize and initially coalesce into short linear chains due to attractive interparticle magnetic dipole interactions. Diffusion slows as the chains extend and continue to coalesce, primarily at chain ends. Fig. 1b shows chains formed after 50 s of field exposure at concentrations 10^{10}/mL. The chains are all located on the slide surface, and no free particles remain in solution. The vertical confinement arises from the vertical gradient of the magnetic field, which results in an equilibrium concentration [16,17] of the form $C(z)\sim\exp(-z/z_o)$ where $z_o = k_BT/(N\ m\nabla H)$. Here, the energy has been expanded to first-order in the z coordinate, k_BT ($\sim 4\times10^{-14}$ ergs) is the Boltzmann energy, m is the nanoparticle moment ($\sim10^{-13}$ emu), ∇H ($\sim$1 kOe/cm), and N the

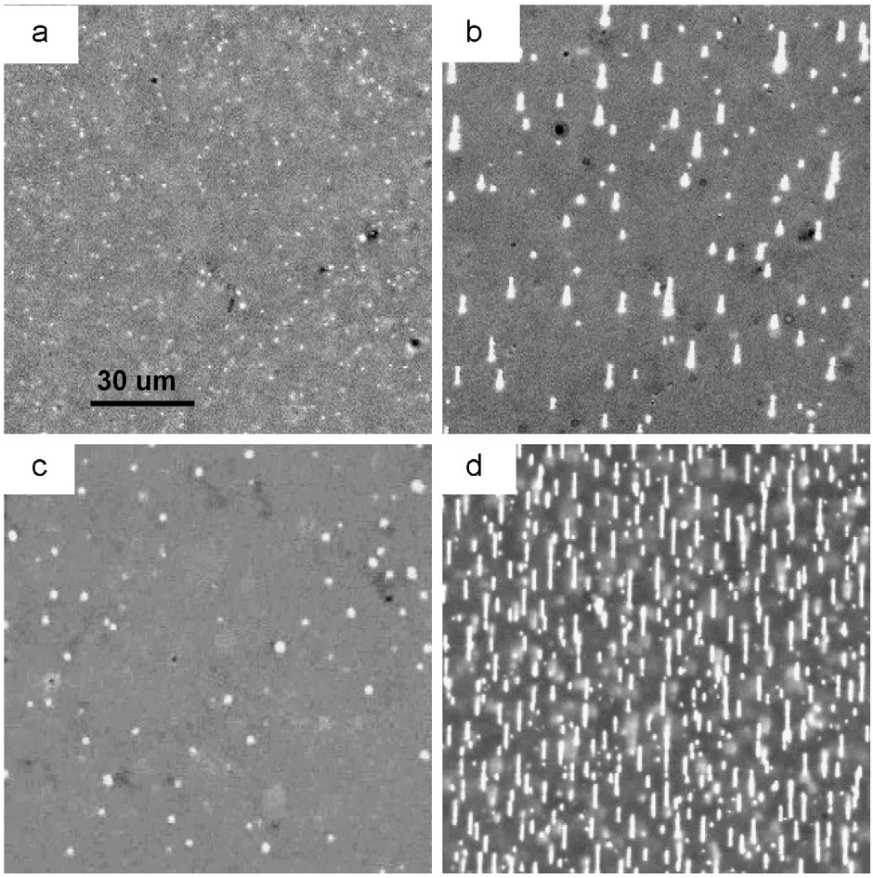

Fig. 1. (a) Images of SAF nanoparticles in a 20 μm deep chamber slide in zero field and at 10^{10}/mL initial concentration. (b) Chain structures formed 50 s after H was increased to 1 kOe, 10^{10}/mL. (c) Small chains which form under the same conditions, except the concentration is 10^9/mL. (d) Numerous chains formed in 15 s when the concentration is 10^{11}/mL.

number of particles in a chain. Since $z_o \sim 10/N\mu m$, single particles in 20 μm deep cells are moderately effected by the vertical gradient while long chains are strongly localized at the surface. Chains formed at a reduced concentration 10^9/mL are shown in Fig. 1c. Coalescence is slower here because diffusion must carry particles and chains over longer distances to attain proximities where the attractive interparticle magnetic dipole–dipole interactions become comparable to k_BT, so that capture is probable. The maximum interparticle interaction energy can be estimated using the field produced by a spherical dipole, of diameter d, at the center of an identical particle with which it is in contact. This yields $E = -2\,m^2/d^3 \sim -2 \times 10^{-11}$ ergs at saturation, whose magnitude is five hundred times larger than k_BT. Interparticle interaction energies are thus comparable to thermal energies at separations of $10d \sim 1\,\mu m$. Thermal diffusion dominates at larger separations, limiting the aggregation rate at low concentrations. At a higher concentration, 10^{11}/mL, Fig. 1d shows that chains rapidly and reversibly form into fairly dense deposits about 10 s after the field is applied. At these concentrations, where 1 mm thick solutions contain a monolayer of nanoparticles, chains are dense enough that they contact and bind in a side-to-side fashion. Such lateral growth of chains is well known and is generally associated with short range interactions which optimize attractive intra-chain dipole–dipole interactions by positioning the nanoparticles of one chain in the notches of the second chain, whence magnetic interactions of near neighbors are all attractive [7]. These interactions are important in that they, along with the longer range interactions of the dipole moments of chains and diffusion, can lead to the formation of composite chains whose mean diameter is not limited to a single particle diameter.

At 10^{10}/mL concentrations, chains usually remain mobile on the slide surface for hours, continuing to aggregate and gradually becoming attached to the slide surface. Fig. 2a shows chains formed at 10^{10}/mL, from the same run as Fig. 1b, after remaining in 1 kOe field for 10 min. This image includes dark points, which mark the digitized coordinates of the endpoints of selected chains at 10 s intervals thereafter, to display the ongoing motion. Although these chains appear quite stable, aside from diffusion and growth, they rapidly disintegrate when the applied field is removed, provided the nanoparticles have been properly treated with passivating surfactants. Fig. 2b shows the initial disintegration of chains, also seen intact in Fig. 2a, a few seconds after removal of the magnet. Untreated particles often only partially fragment into shorter chains, which undulate and rotate when the field is removed. The continuing motion of chains on the surface, in the absence of lateral field gradients or flow, represents diffusion due to thermal excitation which is constrained by viscous drag of the liquid near the slide surface and possible frictional interactions with the slide. This motion is informative because diffusion constants in viscous solutions are of the form [18] $D_i = kT_B/f_i$, where f_i is the viscous drag coefficient in Stokes viscous drag force $F_S = f_i v_i$, with v_i the drift velocity. To measure effective chain diffusion constants, the short time rms displacements of chains, during a time interval of n frames, are averaged over an individual chain trajectory and are found to fit $t^{1/2}$ dependences. The results show a qualitative agreement with the expectation that long chains generally diffuse more slowly, but the scatter in the data (not shown), suggests that

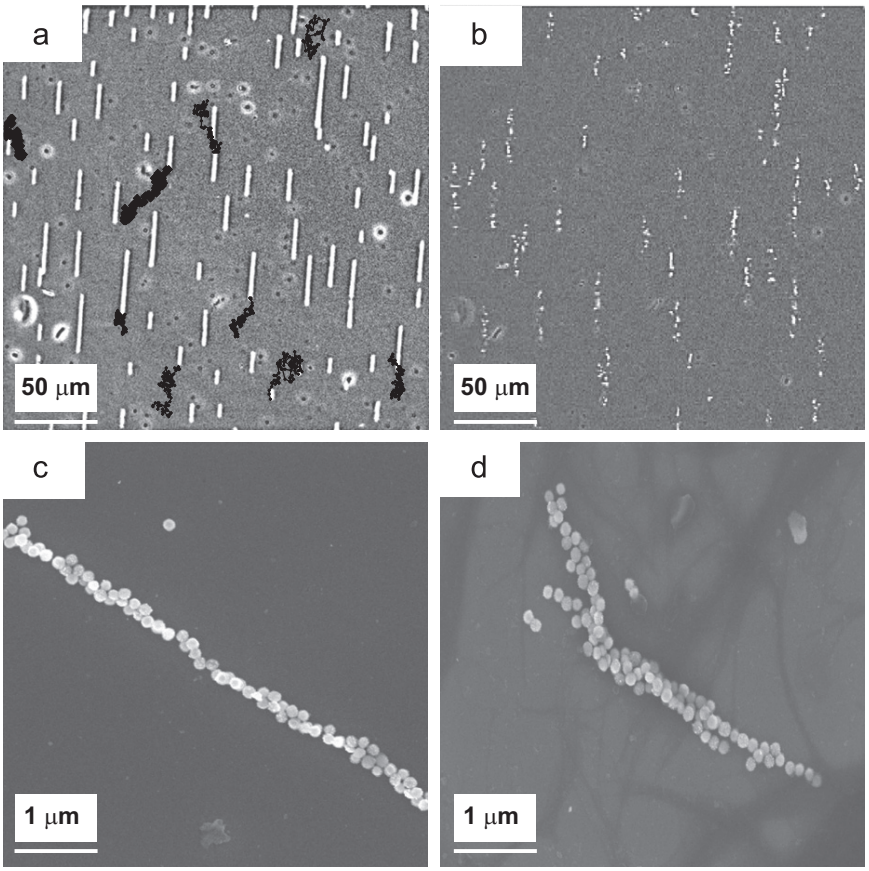

Fig. 2. (a) Image showing chains formed with 10^{10}/mL after 10 min. Black dots show selected chain endpoint positions at 10 s intervals, indicating substantial chain diffusion. (b) The chains in (a) begin disintegrating seconds after the applied field is removed. (c) SEMs reveal that chains are not ideal single particle filaments, and that some chains appear to be composites formed from several chains.

other variables also play a significant role. To evaluate this possibility, SEM was used to examine chains which were formed on a warm magnetic hotplate during solution evaporation. Fig. 2c shows a slender chain, which is nonetheless not a simple line of particles, while Fig. 2d shows a more complex structure which may have resulted from the lateral fusion of a few narrow chains. It thus appears likely that complex internal chain structure is one cause of scatter, and that efforts to better understand and control chain heterogeneity are perhaps more valuable than extensive statistical analysis.

In the presence of a magnetic force $F_m = -\nabla(m \cdot H)$, the magnitude of magnetophoretic velocity is $v_i = \nabla(m \cdot H)/f_i$. Since magnetic forces scale as the number of particles in the chain, it might be hoped that the narrow dimensions of chains would result in small viscous drag and very rapid magnetophoresis. The appropriate viscous drag coefficient for chains can be estimated by considering analytical formula derived for elongated ellipsoids. For an ellipsoid, of length L and diameter d with $L/d \gg 1$, moving along its long axis in a fluid with viscosity η, Berg [18] gives $f_e \sim 2\pi\eta L/\ln(L/d)$, as compared to $f_s = 3\pi\eta d$ for a sphere. Since the magnetic force on the ellipsoid scales as Ld^2, one anticipates that magnetic mobility increases only logarithmically with chain length for ellipsoidal shapes. This is in strong contrast with the case of spheres whose velocities increase as r^2. However, the chain diameter d also enters f_e logarithmically, but appears as d^2 in the magnetic force. Thus, the formation of compact composite chain structures, resembling spheres, can lead to significant magnetic mobility increases.

Chain translations induced by lateral field gradients can be viewed using digital multiple exposures, as exemplified by Fig. 3a. The extended objects in this image are chain trajectories and accurate chain lengths and displacements can be deduced from the digital images. An alternative method to depict chain motion is to rotate the applied lateral field gradient and determine the magnetophoretic velocity from the radius of the resulting circular arcs. Fig. 3b shows the initial chain positions and lengths for a sample which has become quite heterogeneous over the course of hours of measurements, but which conveniently displays the variation of chain velocity with length. Fig. 3c shows the chain trajectories induced by rotating the magnet. Inspection of this image shows that there is correlation between chain lengths and trajectory radii, but also that some chains appear to be susceptible only to rotation, forming rosettes as they rotate about surface attachment points while being refractory to gradient-mediated magnetophoresis. In addition, brighter chains appear to move more rapidly, which is consistent with increased contrast and mobility for thicker chains. Overall, we see 10-fold variations of radii for such extremely heterogeneous samples. These images also make it clear that induced chain rotations and broad magnetic velocity distributions will naturally lead to chain collisions. Lateral binding of chains driven into contact by these magnetic manipulations is frequently observed and substantially increases the chain polydispersity. Thus, chain characteristics depend on the detailed history of the methods used for chain formation and manipulation. One interesting method to gain better control of chain homogeneity is to orient the magnetic field vertically, in which case the chain length is limited by the optical cell depth. When chains extend across the cell, the dipoles at their ends always interact in a repulsive mode which helps to prevent lateral chain aggregation. The optical contrast of vertical chains,

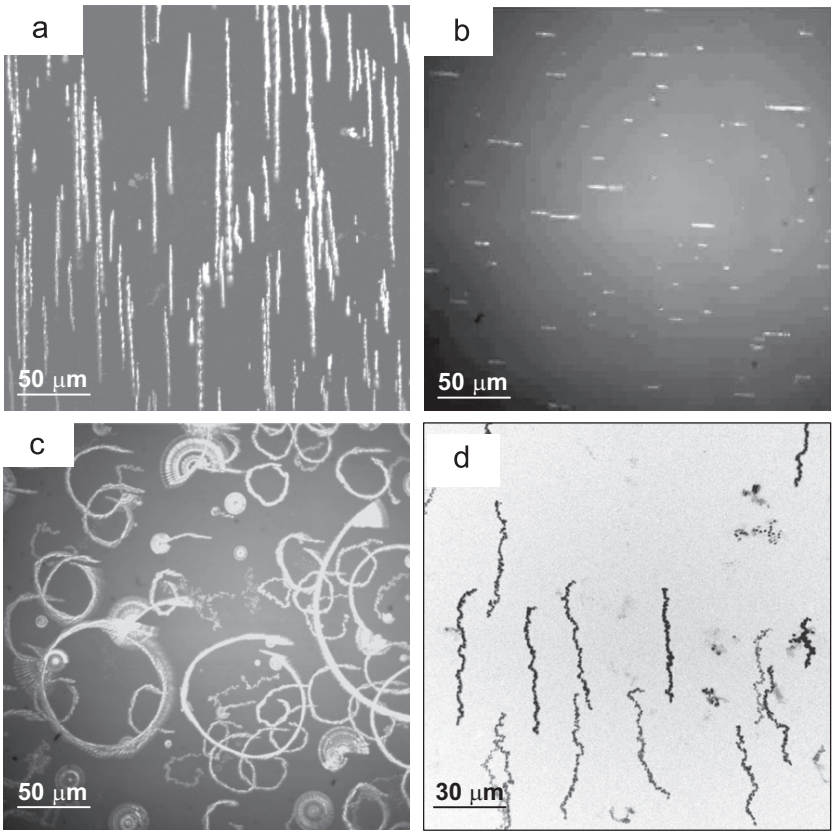

Fig. 3. (a) Chain trajectories during gradient driven magnetophoresis are rendered using digital multiple exposures. (b) Initial view of chains in an aged sample, where the magnet is rotated to create circular magnetophoretic trajectories shown in (c). Some chains are susceptible to rotations about fixed surface binding points, but are not free to translate. (d) Vertical orientation of chains in thin cells alters optical contrast, making vertical chains appear dark, and limits chain length and mobility heterogeneities.

with the focus set at the slide surface, is altered since scattered light is defocused and lost, so that vertical chains appear dark relative to background scattering. Fig. 3d shows an example of magnetophoretic trajectories of chains formed in this way, and dispersion of trajectory lengths is clearly greatly reduced. Although this method appears to improve chain monodispersity, rotating these chains to in-plane orientations results in rapid end-to-end chain growth. Vertical rotations can also result in breakage of chains which are longer than the cell depth. Careful consideration of many factors will be necessary to evaluate possible performance advantages of vertically oriented chains.

We found that several magnetic biological reagents, including MagCellect nanoparticles for bio-separation, also form optically observable chains. These nanoparticles have relatively high FeOx content ($>50\%$) and diameters near 100 nm, but their light scattering is insufficient to allow us to observe individual particles in bright field. Fig. 4a shows a composite image displaying the contrast of bright metallic SAF and faint MC chains in adjacent droplets in the same chamber slide. The MC chains form at low fields of 100 Oe, which is desirable for separation in modest fields, while the chain formation field of the metallic nanoparticles was deliberately adjusted to require much higher fields (500 Oe), by using multiple $Co_{90}Fe_{10}$ multilayers and thin, strongly antiferromagnetic coupling Ru layers. The film structure for these particles is 5 Ta/2 Ru/2 $Co_{90}Fe_{10}$/ (0.6 Ru/2 $Co_{90}Fe_{10}$)$_3$ /2 Ru/5 Ta. Particles with this structure have saturation fields near 2 kOe, but form chains at 500 Oe when the nanoparticles are approximately 25% magnetized. To better understand interparticle interactions, we examined mixtures of MC and SAF nanoparticles and found that they are transformed [15], at 100 Oe, into mixtures of chained MC coexisting with unchained SAF, as demonstrated in Fig. 4b. When the field is further increased the SAF deplete from the solution and condense on, and brighten, the pre-existing MC chains, Fig. 3c. The SAF are then released from the MC chains by reducing the field to 100 Oe, whereupon the region in Fig. 4c rapidly transformed into that shown in Fig. 4d. It is thus seen that using distinctive magnetic particles allows the magnetically staged formation of composite chain structures. This type of manipulation allows field programmable release of selected magnetic nanoparticles, and their payloads, from chains whose cores are comprised of particles which coalesce at lower fields. The low-field chain structures may confer advantages associated with their size- and shape-dependent transport behavior. Similarly, if one uses enhanced chain mobility [19] or size effects [20] to extract or retain chains formed at low fields, then one can, in principle, subsequently increase the field to chain and separate the remaining particles, demonstrating a multiplex separation.

These phenomena can be qualitatively understood by considering the interparticle dipole–dipole interaction energies which determine initial chain formation. The magnitude of the saturated dipole–dipole interaction of spherical particles is roughly $2(m_{MC})^2/d^3$ and $2(m_{SAF})^2/d^3$, respectively, where m and d are the particle saturation moment and diameter, respectively, and the particles are assumed to align, in contact, along the field direction. These interaction energies must be comparable to k_BT to allow chain formation at the chaining fields of 100 and 500 Oe, respectively, implying that the magnetic moments of these MC and SAF (at 100 Oe) differ by roughly a factor of two. It is also

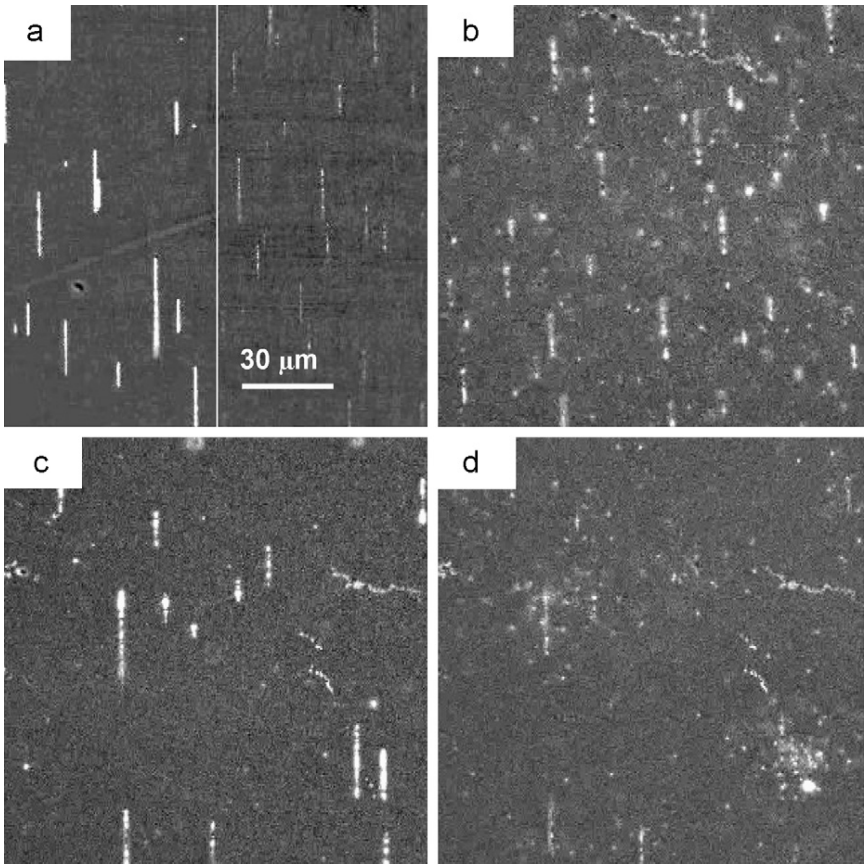

Fig. 4. (a) Composite image showing bright contrast of metallic nanoparticle chains (left) and fainter chains of MagCellect chains (right) in the same cell. (b) At 100 Oe, the MC particles chain while the high saturation field metal nanoparticles diffuse rapidly. (c) When the field is increased, SAF particles attach to the chains, brightening them and depleting bright isolated nanoparticles. (d) When the field is reduced to 100 Oe, the metal particles detach.

apparent that the mixed particle interaction energy, $2m_{MC}m_{SAF}/d^3$, has a value intermediate between those of homogenous particles. Thus, one expects that low-field chains will be active nucleation sites for condensation of the particles which self-chain only at high fields. This suggests that binding of SAF at complex sites at the ends and along the body of low-field (MC) chains is probable, if the field is insufficient for formation of SAF chains. Although this process can, in principle, be repeated for multiple separations, these simple arguments do not account for the complex binding and coordination effects which must be expected for composite chains. Further empirical work, using sets of distinguishable particles will be required to determine the extendibility of such methods.

To observe interactions of chains with immuno-magnetically labeled cells, a mixture of labeled cells and magnetic nanoparticles was pipetted into a sub-mm-thick drop on a microscope slide. Cells settle fairly rapidly on the slide, much faster then even dense nanoparticles. This is to be expected since the gravitational sedimentation velocity is $v_s = (\delta\rho)d^2a/6\eta$, where $\delta\rho$ is the density difference, d is the diameter, a is the acceleration, and η is the viscosity. This formula yields cell settling velocities (at 1 g) of tens of μm/s, while dense ($\delta\rho = 10$ g/cc) 100 nm nanoparticles settle at 0.2 μm/s. In solutions containing unbound magnetic nanoparticles, magnetic chains assemble on the cell-decorated slide surface in minutes, as shown in Fig. 5a. Initially, the chains do not appear to interact with the cells, as the chains may be rotated or translated with no effect on the cells. However, over some minutes of incubation, the chains magnetically link to the labeled cells, which are then easily rotated and translated by the large attached chains. The magnetic linkage of chains and cells is clearly demonstrated in higher resolution image streams [15], as illustrated in Fig. 5b. Here, cells and chains are evident, and a counterclockwise in-plane rotation of the field induces the same rotation in the cells, as shown in Fig. 5c. The magnetic field can also be repeatedly rotated out-of-plane, inducing a corresponding end-over-end rotation of the chain–cell assemblies, which leads to fairly rapid lateral translation. Fig. 5d shows the same region after a few cycles of out-of-plane rotations has translated the cells by a few cell diameters, and cumulative motion on the mm scale is readily obtained. Chains are not apparent in this image because they are oriented vertically and present reduced optical contrast. Finally, these magnetic handles conveniently disintegrate when the magnetic field is removed, especially for fresh samples. This reduces the required cell surface coverage of magnetic nanoparticles and related nanoparticle induced anomalies, such as strong optical side scattering. Because chains have lengths of tens of microns and widths which may be several nanoparticle diameters, each chain is comprised of thousands of nanoparticles and can generate forces larger than the surface loading of antibody bound particles. This transient magnetic amplification might be especially useful for weakly expressed surface antigens, or when high separation velocities are desired.

These broad results show that chain formation is common for 100 nm magnetic nanoparticles. Many details of magnetic chain formation and responsiveness have been observed for metallic nanoparticles, and extension to smaller or non-metallic particles will be possible with adequate dark field illumination. The strong increases of magnetic torques and forces, produced by assemblies containing thousands of nanoparticles, lead to enhanced magnetophoretic velocities which are limited by relatively large viscous drag forces on non-compact chain structures. Control of the structure of three-dimensional chains, which eludes our optical characterization, could be helpful for much larger mobility enhancements. The strong and anisotropic forces on chains interacting with cells may also play important roles in magnetic transfection and targeting and strong interparticle interactions in

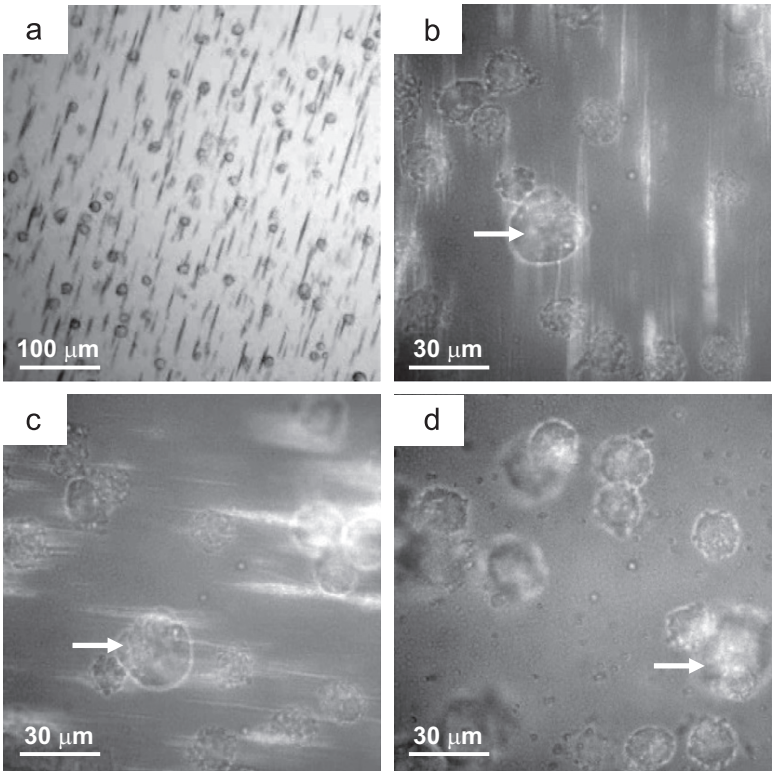

Fig. 5. (a) An image showing MagCellect chains which form on a slide surface that is covered with settled immuno-magnetically labeled cells. (b) A higher magnification view shows cells interacting with chains. (c) Rotation of the magnetic field in the slide plane leads to corresponding rotations for cells attached to chains. (d) Out-of-plane rotations produce an end-over-end motion of chain-cell assemblies, resulting in lateral translations. Arrows mark the same cell in different frames.

clustered materials may also be of advantage for hyperthermia. Finally, our ongoing observations of nanoparticle interactions at higher concentrations or with thin film magnetic structures reveal a wealth of fascinating ferrofluid-like phenomena which we will continue to investigate.

Acknowledgements

This work was supported by grants from NIH (1U54CA119367-01). We also acknowledge the use of the Stanford Nanofabrication Facility, partially supported by NSF, and the Stanford Nanomagnetics Facility. Aihua Fu acknowledges support from NIH pathway to independence award (1K99EB008558).

References

[1] M. Zborowski, J.J. Chalmers, (Eds.), Magnetic Cell Separation, in Laboratory techniques in biochemistry and molecular biology 32, 2007.
[2] J.M. Perez, L. Josephson, R. Weissleder, Chem. BioChem. 5 (2004) 261.
[3] G.X. Li, V. Joshi, R.L. White, et al., J. Appl. Phys. 93 (2003) 7557.
[4] M. Kettering, J. Winter, M. Zeisberger, et al., Nanotechnol. 18 (2007) 175101.
[5] M. Muthana, S.D. Scott, N. Farrow, et al., Gene Ther. 15 (2008) 902.
[6] S.W.K. Chapman, P.O. Hassa, S. Koch-Schneidemann, et al., J. Magn. Magn. Mater. 320 (2008) 1517.
[7] E.M. Furst, A.P. Gast, Phys. Rev. Lett. 82 (1999) 4130.
[8] B. Rabquer, A.K. Shriner, S.L. Smithson, et al., Vaccine 25 (2007) 2036.
[9] F.A. Cardoso, J. Germano, R. Ferreira, et al., J. Appl. Phys. 103 (2008) 07A310.
[10] L. Kostura, D.L. Kraitchman, A.M. Mackay, NMR Biomed. 17 (2004) 513.
[11] W. Hu, R.J. Wilson, A.L. Koh, et al., Adv. Mater. 20 (2008) 1479.
[12] W. Hu, R.J. Wilson, L. Xu, et al., J. Vac. Sci. Technol. A 25 (2007) 1294.
[13] A.L. Koh, W. Hu, R.J. Wilson, et al., Ultramicroscopy 108 (2008) 1490.
[14] A.L. Koh, W. Hu, R.J. Wilson, et al., Philosophical Magazine 88 (2008) 4225.
[15] Selected illustrations and videos available at 〈http://www.stanford.edu/group/wang_group/video/〉.
[16] P. Mulder, G. Molema, S. Koster, et al., Proc. 2006 Int. Conf. Microtech. Med. Bio. (2006) 155.
[17] R.E. Rosenzweig, Ferrohydrodynamics, Cambridge University Press, New York, USA, 1985.
[18] H.C. Berg, Random Walks in Biology, Princeton University Press, Princeton, NJ, USA, 1993.
[19] C.T. Yavuz, J.T. Mayo, W.W. Yu, et al., Science 314 (2006) 964.
[20] F. Lacharme, C. Vandevyver, M.A.M. Gijs, Anal. Chem. 80 (2008) 2905.